Journal of Microscopy, Vol. 215, Pt 3 September 2004, pp. 281–296
Received 6 February 2004; accepted 10 May 2004

Minimizing photobleaching during confocal microscopy of fluorescent probes bound to chromatin: role of anoxia and photon flux

T. BERNAS*,†, M. ZARĘBSKI*, P. R. COOK‡ & J. W. DOBRUCKI*

**Laboratory of Confocal Microscopy and Image Analysis, Department of Biophysics, Faculty of Biotechnology, Jagiellonian University, Gronostajowa 7, 30-387 Krakow, Poland*

†Department of Plant Anatomy and Cytology, Faculty of Biology and Environmental Protection, University of Silesia, Jagiellonska 28, Katowice, Poland

‡Oxford University, Sir William Dunn School of Pathology, South Parks Road, Oxford OX1 3RE, U.K.

Key words. 3D image reconstruction, chromomycin A_3, eGFP, imaging, oxygen, propidium iodide.

Summary

Exposure to light can destroy the ability of a molecule to fluoresce. Such photobleaching limits the use of fluorescence and confocal microscopy in biological studies. Loss of fluorescence decreases the signal-to-noise ratio and so image resolution; it also prevents the acquisition of meaningful data late during repeated scanning (e.g. when collecting three-dimensional images). The aim of this work was to investigate the role of oxygen in the photobleaching of fluorophores bound to DNA in fixed cells, and to explore whether anoxia could minimize such bleaching. Anoxia significantly reduced bleaching rates and changed the order of reaction of both propidium iodide (an intercalator) and chromomycin A_3 (a minor-groove binder) bound to DNA; it afforded the greatest protection at low photon fluxes. However, it had no effect on the bleaching of the green fluorescent protein (GFP) covalently attached to a histone and so bound to DNA, probably because the protein shielded the chromophore from oxygen. Bleaching of all three fluorophores depended on photon flux. Practical ways of minimizing bleaching were examined, and examples of three-dimensional images of DNA marked by propidium and GFP (collected under standard and optimized conditions) are presented.

Introduction

It is difficult to achieve the spatial resolution that is theoretically attainable using the confocal microscope, especially when imaging biological samples in three dimensions. One major obstacle arises from the fading during image collection of the fluors used to provide contrast. This fading arises from a change in the structure of the fluor caused by the exciting light. The aim of this work was to investigate the kinetics of such photobleaching of fluorescent probes immobilized in the specimen during exposure to the laser in a point-scanning confocal microscope, and to explore whether fading could be reduced by removing oxygen from the sample.

Photobleaching

When a stained biological preparation is illuminated, fluors absorb photons and shift from the ground energy level (S) to the singlet excited energy level (S^*). The absorbed energy is dissipated in a process of radiationless internal conversion, emission of fluorescence, and radiationless intersystem crossing to the excited triplet state T^*. The decay time of S^* is independent of the intensity of exciting light and is about 1–10 ns. The T^* to S transition is forbidden according to selection rules, and so is much slower (about 10^{-6}–10^{-9} s). The molecule in the excited singlet or triplet state may undergo a permanent structural change by reacting with another species (e.g. a dye molecule or oxygen), and the change often reduces the capacity to fluoresce. Reactions between two dye molecules are referred to as the D–D (dye–dye) type (Usui, 1965), and the specific reaction with oxygen is known as the D–O type.

Loss of fluorescence signal is not always due to photodestruction. In some cases a fluor, which has been bound weakly to a cellular structure (e.g. DNA), may dissociate into solution. Because the quantum efficiency of fluorescence of a number of popular DNA probes is significantly lower in solution than in the bound state, dissociation of such probes reduces the

Correspondence: J. W. Dobrucki. Tel.: +48 12 6646382; fax: +48 12 6646902; e-mail: dobrucki@mol.uj.edu.pl

fluorescence of both the structure of interest and the total fluorescence.

The mechanisms of photobleaching during confocal imaging of biological samples are not fully understood (Tsien & Waggoner, 1995). If photochemical reactions were unimolecular or pseudo-unimolecular, bleaching would follow a single-exponential function (Hirschfeld, 1976). Although bleaching reactions in solution typically follow first-order kinetics, the kinetics given by bound fluorophores are more complex (Szabo *et al.*, 1992; Florijn *et al.*, 1995; Patterson *et al.*, 1997; Song *et al.*, 1997; Van Oostveldt *et al.*, 1998; Kunz & MacRobert, 2002). Freely diffusing molecules may have limited access to a bound fluor, and collisions between bound fluors may be infrequent; then, differences in the collision frequency with suitable acceptors probably underlie the different kinetics.

Photobleaching compromises image quality

With a few notable exceptions where photobleaching provides valuable information (Peters *et al.*, 1974; Koppel, 1986; Phair & Misteli, 2000), the loss of fluorescence that accompanies bleaching inevitably decreases the signal-to-noise ratio and so reduces the quality of images obtained by fluorescence microscopy (Pawley, 1995; Stelzer, 1998). If signal loss is severe, it can prevent the acquisition of full data sets; for example, when collecting a succession of images through a sample, or over time. Also, when living cells are imaged, the products arising from bleaching may be toxic to the cell.

Bleaching can be minimized by adding antioxidants (NPG, phenyldiamine, mercaptoethanol, DABCO, cysteine, ascorbic acid, nitroxide free radicals), removing oxygen with glucose oxidase and catalase (Tanhuanpaa *et al.*, 2000), or by shielding the fluor with a bound antibody (Abuknesha *et al.*, 1992). Alternatively, corrections can be made for the effects of bleaching on signal intensity (Nagelhus, 1996).

The role of oxygen in photobleaching

As oxygen is the principal energy acceptor, it seems reasonable to expect that deoxygenation should eliminate D–O reactions and slow bleaching. Experimental data and simulations indicate that anoxia reduces bleaching of fluorescein in solution, without eliminating it (Song *et al.*, 1995). This observation can be interpreted as demonstrating that D–O reactions were not the only ones responsible, and that D–D reactions – and possibly other unknown ones – were involved. One might also imagine that D–D reactions should occur less frequently with bound dye in microscopy, and that eliminating oxygen might then provide even greater protection than in solution.

Gaps in existing knowledge

The mechanism of photobleaching remains obscure, even in the case of fluorescein in solution (Lindquist, 1960; Song *et al.*, 1995). The kinetics, order and mechanism of bleaching of other dyes in solution are even less well understood. Most importantly, almost nothing is known about the photobleaching of fluors bound to biological samples. As a result, it is impossible to design a logical strategy to minimize bleaching. This study attempts to provide information on the role of oxygen in photobleaching in microscopy, and to provide the framework for a rational strategy to minimize it.

Two ways of thinking may be adopted: removing oxygen will increase the lifetime of triplet state and so increase bleaching (Song *et al.*, 1996), or the opposite – removing oxygen will eliminate the predominant (D–O) mechanism of signal loss. Therefore, we wish to establish what role D–O reactions play in a typical microscopy experiment.

Materials and methods

Reagents

Alexa Fluor 488 phalloidin was purchased from Molecular Probes (Eugene, OR), ribonuclease A (RNase), propidium iodide (PI), chromomycin A_3 (CA_3), N-propyl-gallate (NPG) from Sigma-Aldrich (Poznań Poland), Vectashield from Vector Laboratories (Peterborough, U.K.), formaldehyde (16% EM Grade) from Electron Microscopy Sciences (Ft Washington, PA, U.S.A.). NPG solution was made according to (Giloh & Sedat, 1982). Stocks of PI and CA_3 were made in PBS and kept at 4 °C; stocks of RNase were kept frozen. HeLa cells stably expressing histone H2B-eGFP were a generous gift from Dr T. Kanda (Kanda *et al.*, 1998). Compressed argon (BOC Gazy, Poland) was 99.998% pure; the gas was delivered to an imaged sample through copper and steel tubes.

Cell cultures

MSU 1.1 human fibroblasts (Morgan *et al.*, 1991) and HeLa cells were cultured on 20 mm diameter, 0.17 mm thick coverslips (Menzel Gläser, Braunschweig, Germany) placed in tissue culture Petri dishes (TPP, Switzerland). DMEM (Sigma, Poznań, Poland) supplemented with 10% fetal bovine serum (Gibco, U.K.) and antibiotics was used. Confluent monolayers (two days after seeding) were used in all experiments. Cell density was approximately 1100 cells mm^{-2}.

Fixation and fluorescent labelling

Coverslips with live cells were washed three times with PBS (with Mg^{2+} and Ca^{2+}), and fixed with formaldehyde (1% in PBS at 20 °C for 1 h). Coverslips with fixed cell cultures were mounted in a round steel holder using silicone grease. The preparations were incubated in RNase (0.5 mg mL^{-1} in PBS) for 4 h at room temperature and washed three times with PBS. The holder was fitted in a microscope stage microincubator (Life Science Research, Cambridge, U.K.). Nuclei of MSU 1.1

cells were stained by 30 min incubation with a solution of PI (5 μg mL^{-1}) or 25 min with CA_3 (100 μg mL^{-1}) in PBS. Following incubation with PI, the dye solution was removed and the preparation was incubated in fresh PBS for 45 min prior to photobleaching. A rapid exchange of CA_3 ($t_{1/2}$ approx. 3 min) made it impossible to maintain a stable level of fluorescence in the absence of the dye in the incubation solution. Thus, CA_3 was present in the sample throughout the experiment. Fluorescent labelling procedures and photobleaching experiments were carried out at room temperature.

Removal of oxygen

To remove oxygen from samples the microincubator was closed with a glass cover and pure argon was bubbled through the PBS covering the cells for 30 min prior to, and during, image collection. Control experiments with an oxygen-sensitive luminescent probe, $Ru(phen)_3^{2+}$ [Tossi & Kelly, 1989; Dobrucki, 2001), confirmed that oxygen had been removed.

Confocal microscopy

Fluorescence of PI (excitation 488 nm, emission 590–630 nm), CA_3 (excitation 458 nm, emission 490–550 nm) and eGFP (excitation 488 nm, emission 490–550 nm) was detected using a Bio-Rad MRC1024 (Bio-Rad Microscience, Hemel Hempstead, U.K.) confocal system equipped with a Nikon Diaphot 300 microscope, 60× PlanApo oil immersion objective lens (NA 1.4), a 15 mW krypton–argon laser (ALC, Salt Lake City, UT, U.S.A.) and a 100 mW argon ion laser (ILT, Salt Lake City, UT, U.S.A.). Time series of fluorescent confocal images of equatorial sections through nuclei (thickness approx. 1.1 μm) were collected using alternately a small-intensity probing beam and a large-intensity bleaching beam. No measurable bleaching occurred when labels were excited using the probing beam alone. Images (512 × 512 pixels; 256 grey levels) were collected using LaserSharp 3.2 software (Bio-Rad). One image was a sum of 20 (PI), 45 (CA_3) or one (eGFP) consecutive scans. Fluorescence was detected using photomultipliers in photon-counting mode, with electronic amplifier turned on ('Low Signal' on). We found that the dependence between the gain setting and the signal amplitude was linear. The amplitude of the measured PMT signal was amplified approx. 12.5×.

The intensity of exciting light was adjusted using neutral density filters. The total values measured at the entrance pupil of the objective, using LaserCheck light meter (Coherent, Santa Clara, CA) were: 0.02–0.6 mW and 0.007 mW (GFP bleaching and probing beam, respectively); 0.2–2.0 mW and 0.02 mW (PI bleaching and probing beam, respectively); 0.33–3.3 mW and 0.03 mW (CA_3 bleaching and probing beam, respectively). These total intensities were divided by the total area of the image to obtain the average fluxes of excitation light given in the figures and tables. The light was focused approximately 0.8 μm above the surface of the oil-coupled coverslip, in the water medium. Thus, the effective numerical aperture was assumed to be 1.23. Consequently, the instantaneous fluxes of exciting light (averaged over the area of the first maximum of the Airy disc) were: 8.3–250.5 kW cm^{-2} and 2.5 kW cm^{-2} (GFP bleaching and probing beam, respectively); 83.5–834.8 kW cm^{-2} and 8.3 kW cm^{-2} (PI bleaching and probing beam, respectively); 133.5–1335.7 kW cm^{-2} and 13.36 kW cm^{-2} (CA_3 bleaching and probing beam, respectively). During image registration the sample was in equilibrium with atmospheric air or argon, as indicated. Experiments were performed three to six times in each set of conditions and 45–90 nuclei were analysed.

Analysing kinetics of photobleaching

Time series of 2D image stacks were converted to sets of 8-bit uncompressed tiff files (one set per detection channel), transformed back to the form of stack with Matlab 5.2 and pre-processed using a median filter (square mask 3 × 3). Only pixels with an initial brightness of ≥ 6 on the grey scale were analysed. The grey scale was subdivided into 25 consecutive intervals (i.e. from 6 to 15, 16 to 25, etc.) using binary masks. Average intensities of pixels comprising each brightness class were calculated for each of the images in the stack, before background (the mean intensity of signal in an area without cells) was subtracted. These corrected values were plotted against the total dose (J cm^{-2}) of the incident light and the number of scans (Figs 1–4).

Calculation of bleaching rates and apparent reaction orders

The method used was adapted from (Patterson & Piston, 2000). In the first step, bi-exponential functions, described by the following general equation:

$$I(w) = Ae^{-Bw} + Ce^{-Dw} \tag{1}$$

where I is fluorescence intensity, w is total incident excitation light dose and A, B, C and D are phenomenological coefficients, were fitted to kinetic curves using the Marquart–Levenberg algorithm (SigmaPlot 6.0). Subsequently the initial absolute rates of photobleaching (R_a is loss of fluorescence measured in arbitrary units divided by light dose) were calculated using the first derivatives (taken at 0) of the fitted functions (Eq. 1):

$$R_a = \left.\frac{dI}{dw}\right|_{w=0} = AB + CD. \tag{2}$$

Alternatively, where it was not possible to fit a bi-exponential function (the fast phase of photobleaching of PI) the absolute photobleaching rate was approximated using the following formula:

$$R_a = \frac{(I_0 - I_1)}{\Delta W_1}, \tag{3}$$

where ΔW_1 is the respective excitation dose of one set of bleaching scans (image).

Where indicated, the relative rates of photobleaching were used:

$$R_r = \frac{R_a}{I_0} \tag{4}$$

The following, general equation was assumed to describe the photobleaching reaction:

$$-\frac{d[F]}{dt} = k_b[F^*]^\alpha, \tag{5}$$

where F and F^* are concentrations of non-bleached fluorophore in the ground and excited states, respectively; k_b is the bleaching constant (proportional to absoption cross-section and quantum efficiency of the bleaching reaction); α is the apparent order of photobleaching reaction.

Substituting Eqs (2)–(5) one obtains:

$$-\frac{d[F]}{dt} = a\frac{dl}{dw}\frac{dw}{dt} = aR_aJ = k_b[F^*]^\alpha, \tag{6}$$

where a = constant, J = excitation light flux and R_a = absolute rate of photobleaching.

The concentration of the excited fluorescent label (F^*) is proportional to the concentration of the nonbleached label in a given voxel (F) and excitation light photon flux (J). Consequently, the apparent order of photobleaching reaction (α) was calculated from the slope of the plot of ln $R_a{}^*J$ against J:

$$\ln(R_aJ) = \alpha \ln(J) + \ln(b), \tag{7}$$

where b = constant and J = light excitation flux.

In the experiments where CA_3 was used, a constant (equilibrium) level of fluorescence was obtained after the first few scans with a bleaching beam, due to a rapid exchange of the dye with solution. Therefore, calculation of the initial rate of photobleaching (using the method described earlier) was not possible. Instead, the logarithm of the loss of fluorescence was plotted against the level of remaining fluorescence at equilibrium. Subsequently a photobleaching constant and an apparent order of the reaction were calculated from ln–ln plots (as described in Materials and Methods).

Modelling the signal-to-noise ratio

As photon-counting was used, the intensity of fluorescence signal was assumed to be proportional to the number of photons. On the other hand, the background comprised Poisson noise, dark current (proportional to integration time) and constant readout noise. Hence, the signal-to-noise ratio was defined as:

$$s/n = \frac{N}{N^{1/2} + bt_f + r} \tag{8}$$

The number of photons (N) emitted by a collection of fluorophore molecules (Eq. 8) was calculated from Eq. (5) by double numerical integration with respect to time (from 0 to t_f), using routines of Derive 3.3. The dark current coefficient (b) was set to 1 and readout noise to 10, respectively. s/n was plotted as a function of integration time (t_f) and the flux of excitation light (which affected both a bleaching constant k_b, and fluorescence signal intensity, I).

Analysis of heterogeneity of kinetics of photobleaching

In order to distinguish contingent, spatially separated, populations of pixels (regions) differing with respect to the kinetics of photobleaching, fluorescence bleachmaps were constructed as described in Brakenhoff *et al.* (1994). Briefly, two images, one collected prior to, and the other collected following the photobleaching session, were compared. The two images were collected using a small-intensity nonbleaching probing beam. The bleaching was achieved with several scans of a large-intensity laser beam. In control experiments the probing beam was used instead of the bleaching beam. Fluorescence intensities of all pixels in the first image were plotted against the intensities of corresponding pixels in the second image. Distinct populations of pixels differing with respect to kinetics of photobleaching manifest themselves as separate groups of points in such dot-plots (bleachmaps) (Brakenhoff *et al.*, 1994). Linear functions were fitted to the bleachmaps and distributions of deviations of the points from the regression line (residuals) were constructed using bins of 20 fluorescence intensity units. The respective distributions obtained for bleaching experiments were compared with the distribution of the control using the Chi-square test (d.f. = 24).

Calculating photobleaching rates of CA_3

It was assumed that the constant fluorescence intensity of CA_3 was a result of reaching equilibrium between the increase (due to illumination) and decrease (due to dissociation from DNA) of bleached fluorophore.

$$\frac{d[B]}{dt} = k_b[F]^\alpha - k_d[B] = 0. \tag{9}$$

where k_b is the photobleaching constant; k_d is the dissociation constant; and $[B]$ and $[F]$ are concentrations of bleached and nonbleached fluorophore, respectively.

Therefore, substituting:

$$[B] = [F_0] - [F] \tag{10}$$

into Eq. (9) one obtains:

$$k_b[F]^{\alpha} - k_d([F] - [F_0]) = 0 \qquad (11)$$

Hence, as fluorescence intensity is proportional to the concentration of nonbleached fluorophore:

$$\alpha \ln(I) + \ln\left(\frac{k_b}{k_d}\right) = \ln(I - I_0) \qquad (12)$$

Consequently, the apparent order of bleaching reaction and the relative bleaching constant were calculated from the ln–ln plots of the equilibrium fluorescence intensity vs. the loss of the intensity at equilibrium.

Results

Oxygen-dependent photobleaching of Alexa 488

Fluorescein-labelled cell structures are photobleached rapidly by the exciting light during fluorescence microscopy. We first studied bleaching of Alexa 488 conjugated to phalloidin and bound to actin in fixed human fibroblasts. Alexa 488 is a fluorescein derivative known for its higher photostability. Anoxia reduced bleaching significantly (data not shown), much as it does with fluorescein (Song *et al.*, 1995). This suggests that anoxia may provide a useful way of reducing bleaching. Therefore, we analysed the effects of anoxia on the kinetics of bleaching of some fluorescent probes commonly used to investigate chromatin.

Three fluorophores which bind in different ways to chromatin were studied: propidium iodide (PI) – a DNA intercalator, chromomycin A_3 (CA_3) – a DNA minor-groove binder, and an enhanced version of the green fluorescent protein (eGFP) covalently attached to histone H2B, which is incorporated into nucleosomes that bind to DNA. The rates of bleaching of these fluorophores bound to chromatin in fixed cells were investigated under air or argon, and analysed as a function of the local fluorophore concentration and flux of exciting light.

Photobleaching of propidium iodide

The main binding mode of PI is through intercalation, which unwinds the double helix by 26° (Blackburn & Gait, 1996). The dye binds stoichiometrically, and the binding constant is unaffected by chromatin condensation or base composition (Araki & Yamada, 1985; Darzynkiewicz & Kapuscinski, 1990). The fluorescence quantum yield of PI increases ~20-fold on binding (Cosa *et al.*, 2001). The excitation/emission spectra and fluorescence quantum efficiency after binding double- or single-stranded DNA are similar (Cosa *et al.*, 2001). As the binding constant of intercalated PI is so high, the bound dye does not dissociate detectably from DNA during the experiments described here.

Fixed cells were treated with RNase to remove RNA, stained with PI, and scanned using a confocal microscope; then groups of successive scans were used to generate images. As expected, PI marked the nuclei in these images. The intensity of fluorescence in the nuclear pixels varied, depending on the amount of chromatin (and so PI) present. For our analysis, we divided the grey scale into 25 classes, ranging from the brightest to the dimmest. For the sake of clarity, we generally present results obtained using only three of these classes – the brightest, medium and dimmest. As nuclei are scanned in air, the intensity of fluorescence declines (Fig. 1A). For the brightest pixels, the decline is biphasic, with an initial fast phase followed by a slower one (Fig. 1A, curve 1). However, this effect becomes progressively less marked with the fainter classes (Fig. 1A,

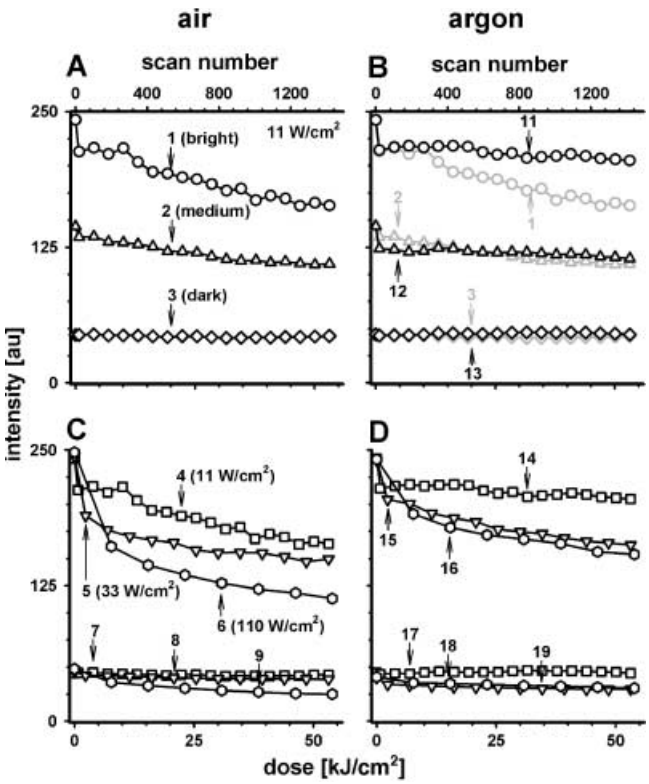

Fig. 1. Kinetics of photobleaching of propidium bound to DNA, in air or argon. Fixed cells were stained with propidium, and equatorial sections scanned with the laser in a confocal microscope under air (A, C) or argon (B, D). Twenty successive scans were accumulated to form one image, and the average intensity (arbitrary units; au) of pixels of different initial brightness in images is plotted relative to the accumulated dose of light. The flux of the incident light is indicated. In each pair of panels, curves 1 and 11, 2 and 12, and so on were obtained in air and argon, respectively; this convention is used in the equivalent pairs of panels in other figures. (A) Bright pixels (curve 1) are bleached more rapidly than darker ones (curves 2, 3). Curves for only three of the 25 brightness classes are shown for clarity. Means of five experiments. (B) Argon lessens photobleaching. Curves 1–3 from (A) are included for comparison with their counterparts (i.e. 11–13) in argon. (C) Effect of three different fluxes on bleaching. Effects on only bright (curves 4–6) and dim pixels (curves 7–9) are shown for clarity. (D) Argon again lessens photobleaching.

compare curves 1, 2 and 3). Under anoxia (i.e. after purging with argon) the kinetics are roughly similar, but the signal intensity falls less rapidly (Fig. 1B, compare curves 1 and 11). This general response is seen with both the brightest and dimmest classes after scanning with light of higher intensities (Fig. 1C, compare curve 4 with 5 and 6, and curve 7 with 8 and 9). It is also seen under anoxia (Fig. 1D). We now analysed the kinetics in these two phases.

PI photobleaching – the initial fast phase

Under air, the fast phase was clearly seen only in the brightest pixels, so pixels with an initial brightness greater than 100 were analysed (Fig. 2A). The absolute rates of bleaching were greater for the brightest pixels (Fig. 2A). These rates were calculated using a linear approximation of a curve, and so were probably underestimates. The normalized bleaching rates were similar for bright and dim pixels (Fig. 2A, inset).

There was only a moderate linear correlation (average $r^2 \approx 0.82$) between logarithms of the absolute rates of bleaching of the brightest pixels and the flux of exciting light (Fig. 2E, left). The apparent order of bleaching was 0.36 ± 0.08 (calculated from the angle between the line and the horizontal axis, for details see Materials and methods). Although it is an underestimate for the reasons given above, this low order of reaction is consistent with the bleaching becoming saturated at high intensities (i.e. no more bleaching occurs).

Under argon, a similar dependence of absolute rates of fast-phase bleaching on initial pixel brightness was observed (Fig. 2B). Absolute bleaching rates were lower than in aerated samples (Fig. 2B and D, compare curve 23 with 33, 22 with 32, 21 with 31), indicating that anoxia protects the dye from bleaching. The apparent average order of reaction for the bright pixels (calculated from data in Fig. 2E) was 0.19 ± 0.06 (average $r^2 \approx 0.84$). This indicates that the saturation of bleaching at high light intensities was more pronounced in anoxia; therefore, oxygen-dependent reactions may contribute significantly to bleaching only at high light intensities.

In order to test whether certain regions of the image differed with respect to the kinetics of bleaching, we compared every pixel in images before and after bleaching (for details of this approach see Materials and methods): no regional differences in the bleach map (in either aerated or anoxic samples) were detected. However, the scatter of the points constituting the maps was greater under all conditions studied than in the control (Table 1). Therefore, it seems plausible that several types of reactions rather than just one contributed to the bleaching process in the fast phase, regardless of the presence of oxygen. Contributions of these putative reactions (reflected in the scatter of the points on the bleachmaps) might be different in the absence and presence of oxygen.

The fast-phase bleaching could result from PI bound to RNA that remained despite treatment with RNase. Therefore, we investigated the kinetics of bleaching of PI bound to RNA in

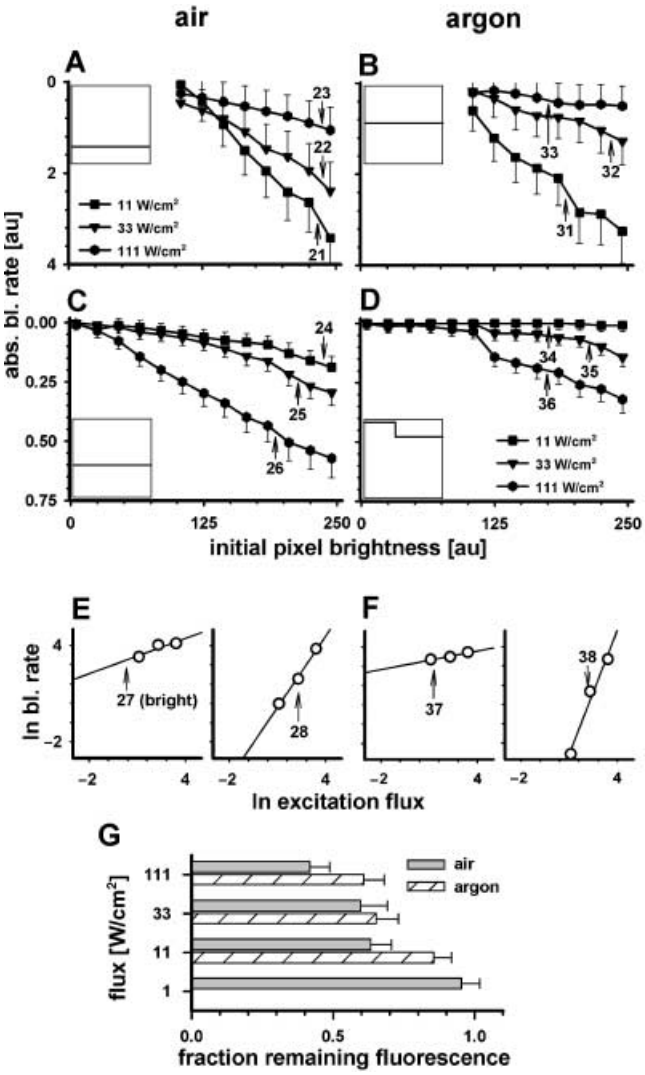

Fig. 2. Analysis of kinetics of photobleaching of propidium bound to DNA in air (A, C, E) and argon (B, D, F). (A), (B) Absolute rates of fast-phase bleaching as a function of initial pixel brightness, for three exciting intensities. Error bars: 95% confidence intervals. Insets: schematics showing normalized bleaching rates as a function of initial pixel brightness. Increasing light intensity brings about a decrease of photobleaching rate, indicating that saturation of this process occurs under air as well as under argon. (C), (D) As (A), (B) for slow-phase bleaching. No saturation occurs, and no bleaching is detectable under low photon flux in argon. (E), (F) Bleaching rates (bright pixels only) for the fast and slow phases (graphs on left and right in each panel, respectively). The order of fast-phase bleaching reactions (determined from the graph as described in Materials and Methods) is well below 1 in air and argon, but high for the slow phase under air (1.5) and even higher under argon (3.2). (G) Fraction of fluorescence remaining on delivery (under air or argon) of the same total dose of light, delivered in laser beams of different photon fluxes. Laser beams of different intensities (i.e. passing through neutral density filters) were used and the total time of illumination was adjusted to deliver the same total dose of light to the sample. Errors bars: 95% confidence intervals. A given dose of light causes less bleaching if delivered at a low photon flux, or under argon.

Table 1. Heterogeneity of photobleaching of PI in the fast phase, based on the bleachmap. Differences between the distribution of magnitude of residuals in illuminated samples and in the control (i.e. a sample illuminated with a nonbleaching dose of light) expressed as Chi-square (significance levels are given in parenthesis).

Excitation light flux (W cm^{-2})	Air	Argon
11	82 (> 0.999)	312 (> 0.999)
33	109 (> 0.999)	131 (> 0.999)
110	43 (> 0.999)	638 (> 0.999)

Table 2. Heterogeneity of photobleaching of PI in the slow phase, based on the bleachmap. Differences between the distribution of magnitude of residuals in illuminated samples and in the control (i.e. a sample illuminated with a nonbleaching dose of light) expressed as Chi-square (significance levels are given in parenthesis).

Excitation light flux (W cm^{-2})	Air	Argon
11	24 (0.42)	71 (> 0.999)
33	43 (0.98)	31 (0.85)
110	365 (> 0.999)	9 (0.001)

nucleoli in preparations that were not subjected to RNase treatment. We found (data not shown) that the rate of signal loss was much slower than that given by the fast phase in Fig. 1(C) and (D). Thus, it is unlikely that the fast phase represents bleaching of PI bound to residual RNA. It seems more likely that ~10% PI binds to DNA in a different way to the predominant binding mode.

PI photobleaching – the slow phase

In oxygen, the absolute rates of slow-phase bleaching increase linearly with initial pixel brightness (Fig. 2C). The slight deviation from linearity, observed for low (curve 24) and intermediate (curve 25) fluxes, was within experimental error. In contrast to the fast phase, no saturation with intensity occurs. There was a linear correlation (average $r^2 \approx 0.96$) between the logarithms of absolute rates of bleaching and the flux of exciting light. The apparent average order of bleaching reactions in the slow phase (over all pixel brightness classes, and calculated from Fig. 2E, right) was 1.5 ± 0.08. This indicates that slow-phase bleaching is not a unimolecular reaction of an excited PI molecule; rather, it depends on several reactions. As for the fast phase, the bleachmap did not reveal any distinct regions with different kinetics of bleaching. Again, the scatter of points constituting the map was significant at high fluxes (Table 2), which is again consistent with more than one reaction contributing to bleaching in aerated samples at high and intermediate fluxes.

For slow-phase bleaching under argon, a different pattern of absolute bleaching rate was observed (Figs 1D and 2D). There was no (or negligible) bleaching in dim pixels (initial brightness < 110), regardless of flux. Moreover, at low fluxes bright pixels (initial brightness > 110) were not bleached. Bleaching was seen exclusively in bright regions illuminated with high or intermediate fluxes. In bright pixels, normalized bleaching rates were independent of initial intensity (Fig. 2D, inset) and, in general, markedly lower under argon than under air (e.g. in Fig. 2, compare curve 26 with 36). Furthermore, protection against bleaching depended on light flux, as discussed below.

For the slow phase under argon, there was a linear correlation (average $r^2 \approx 0.97$) between the logarithms of rates of bleaching of the bright pixels and flux (Fig. 2F, right); the average order of bleaching reactions was 3.2 ± 0.5. As in the presence of oxygen, no distinct regions with different bleaching kinetics were detected in bleachmaps. Only bright pixels, where bleaching occurs, contribute significantly to the scatter of points on the bleachmap; this scatter decreases with increasing flux (Table 2). This supports the notion that – at low fluxes – the slow phase occurs only in bright pixels.

One may postulate that reactions involving oxygen may have an order of 1 (with respect to the concentration excited PI), whereas those involving the dye but no oxygen might be of higher order. The combination of these two types of reactions might then yield lower apparent orders in oxygen.

It seems plausible that there are two classes of PI bound to DNA which interact with oxygen to different degrees. In one, PI molecules interact with oxygen molecules efficiently to give the rapid bleaching, whereas in the other they cannot and give the slow bleaching. Unfortunately, more information about the mechanism and modes of binding of PI to DNA and PI bleaching is required to verify this hypothesis.

Photobleaching of chromomycin A_3

CA_3 binds to the minor groove of DNA either as a dimer (Blackburn & Gait, 1996; Gao & Patel, 1989a,b, 1990) or monomer (Aich *et al.*, 1992; Stankus *et al.*, 1992) complexed with a divalent cation (Mg^{2+}, Zn^{2+}). Binding is unaffected by chromatin condensation. However, CA_3 binds preferentially to G/C-rich DNA (Gao & Patel, 1989a,b). Under our conditions, the dye exchanges rapidly between DNA and the soluble pool, so the bound form can only be maintained in the presence of an unbound pool. Therefore, the loss of DNA-associated fluorescence results from bleaching, dissociation and association of bleached and unbleached molecules. As a consequence of this rapid exchange, a fast initial bleaching is followed by a slower phase, when equilibrium is reached and the signal becomes stable (Fig. 3A–D). Then the intensity of fluorescence remaining is a function of the initial fluorescence intensity and the flux of exciting light. It is reasonable to expect that the association and dissociation constants are unaffected by the intensity of illumination. Thus, the apparent molecularity (order of bleaching reactions with respect to initial brightness) and bleaching constant were calculated at this equilibrium using

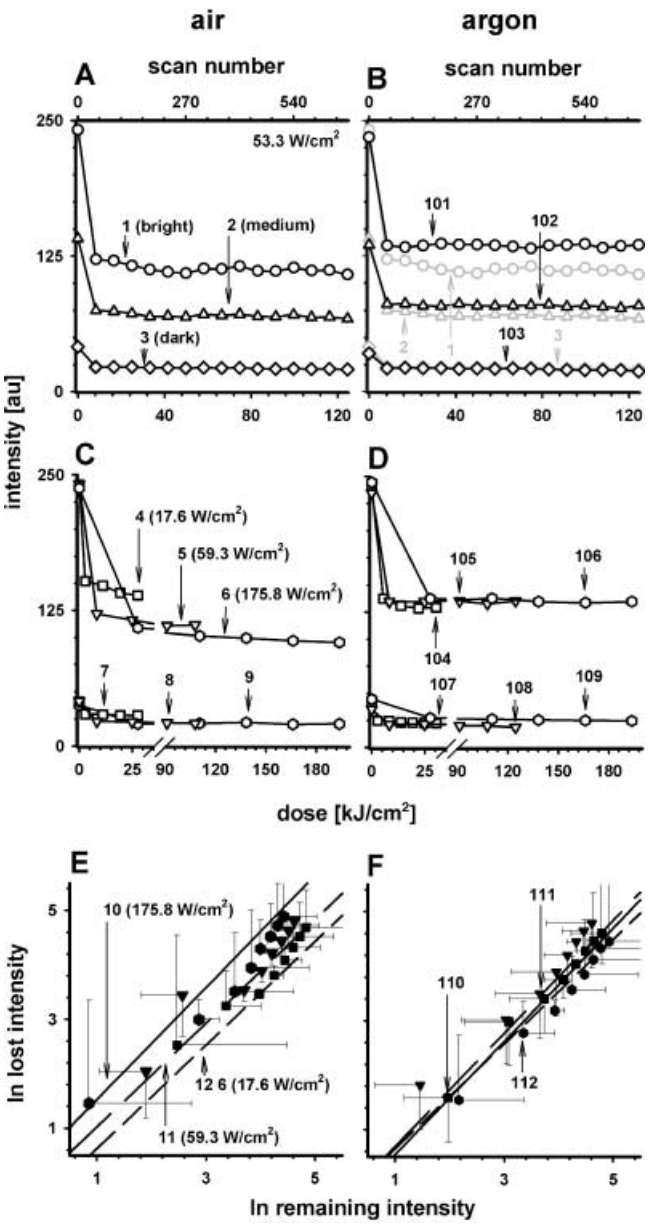

Fig. 3. Kinetics of photobleaching of chromomycin A_3 bound to DNA in air (A, C, E) or argon (B, D, F). The general approach was as described in Fig. 1, except that 45 successive scans were accumulated into one image. (A), (B) Argon has little effect on the initial bleaching. As in Fig. 1(A) and (B), only three brightness classes are shown for clarity, and curves 1–3 in (A) are reproduced in (B). Means of three experiments. (C), (D) Effect of three different fluxes on bleaching. Effects on only bright (curves 4–6, 104–106) and dim pixels (curves 7–9, 107–109) are shown for clarity. Due to a fast exchange of bound and free molecules, the level of fluorescence of DNA-bound label reflects a dynamic equilibrium. Argon increases the equilibrium fluorescence level. (E), (F) Lost fluorescence is plotted against the remaining fluorescence intensity (see Materials and methods). Continuous lines: 175.8 W cm^{-2}. Lines with long dashes: 59.3 W cm^{-2}. Lines with short dashes: 17.6 W cm^{-2}. Error bars: 95% confidence intervals. The reaction order is estimated to be 0.35 in air, and 0 in argon.

Table 3. Relative photobleaching constants (k_b/k_d) of CMA_3 (reaction molecularities in parentheses). Errors represented as 95% confidence intervals.

Excitation light flux (W cm^{-2})	Air	Argon
17.6	0.72 ± 0.12 (0.95 ± 0.10)	0.73 ± 0.15 (0.96 ± 0.10)
52.8	1.07 ± 0.20 (0.95 ± 0.10)	0.70 ± 0.12 (1.04 ± 0.10)
175.8	1.63 ± 0.25 (1.03 ± 0.10)	0.61 ± 0.15 (0.97 ± 0.10)

the plots in Fig. 3(E) and (F). Bleaching appeared to be unimolecular (with respect to CA_3), both in the presence and absence of oxygen (Table 3). The relative bleaching constants did not depend on flux in anoxia, but in the presence of oxygen they increased with flux. We estimated the apparent order of bleaching to be 0.35 ± 0.4 and 0 ± 0.2 in the presence and absence of oxygen, respectively (Table 4). Such a low order of reaction may indicate that bleaching saturates at high intensities. Moreover, bleaching rates were lower in anoxia for high and intermediate fluxes (Table 3; Fig. 3E and F).

Photobleaching of enhanced green fluorescent protein (eGFP)

A gene encoding histone H2B linked to eGFP was expressed in HeLa cells so that the resulting H2B-eGFP protein was incorporated into nucleosomes, and so into chromatin. As a result, the fluorophore is positioned outside the DNA helix and essentially no free eGFP is present in solution. It exhibits a single excitation peak (489 nm) and an emission maximum at 508 nm.

In oxygen, bleaching of eGFP does not follow simple exponential kinetics (Fig. 4A and C); the absolute bleaching rate increases with the flux of exciting light (Fig. 4E). Furthermore, the rate depends on the initial pixel brightness (see Fig. 4E, inset, where rates are normalized). An apparent order of the bleaching reaction of 1.74 ± 0.05 was calculated from Fig. 4(G) (average $r^2 \approx 0.99$). In anoxia, the kinetics were generally similar (Fig. 4B and D); the rate again increased with flux (Fig. 4F), absolute bleaching rates were proportional to initial pixel brightness (Fig. 4F), and the apparent order of the bleaching reaction was 1.66 ± 0.05 (calculated from Fig. 4H; average $r^2 \approx 0.99$). Thus, oxygen does not influence the bleaching of H2B-eGFP, which suggests that it cannot access the chromophore embedded within the protein.

Analysis of the bleachmap again revealed no regional differences (Table 5). Therefore, it seems plausible that the high apparent order of bleaching reaction (> 1) results from multiple excited states of GFP rather than the superposition of reactions of different orders.

Example of anoxic imaging

A summary of all kinetic data and orders of bleaching reactions is given in Table 4. These data indicate that anoxia may

Table 4. Photobleaching rates, and orders of reaction of PI, CMA_3 and eGFP under oxygen and air.

Fluorophore	Excitation light flux ($W\ cm^{-2}$)	Normalized bleaching rate+/ bleaching constant*		Apparent reaction order		Apparent molecularity	
		Air	Argon	Air	Argon	Air	Argon
PI (fast)+	11	0.86 ± 0.20	1.11 ± 0.18	0.36 ± 0.08	0.19 ± 0.06		
	33	0.69 ± 0.10	0.38 ± 0.07				
	111	0.45 ± 0.15	0.20 ± 0.15				
PI (slow)+	11	0.06 ± 0.02	< 0.01 ± 0.01	1.50 ± 0.08	3.20 ± 0.50		
	33	0.09 ± 0.02	0.04 ± 0.01				
	111	0.24 ± 0.04	0.12 ± 0.01				
CMA3*	17.6	0.72 ± 0.12	0.73 ± 0.15	0.35 ± 0.41	0.00 ± 0.20	0.95 ± 0.10	0.96 ± 0.10
	52.8	1.07 ± 0.2	0.70 ± 0.12			0.95 ± 0.10	1.04 ± 0.10
	175.8	1.63 ± 0.25	0.61 ± 0.15			1.03 ± 0.10	0.97 ± 0.10
eGFP+	0.6	0.48 ± 0.46	0.83 ± 0.22	1.74 ± 0.05	1.66 ± 0.05		
	1.7	1.27 ± 0.45	1.08 ± 0.31				
	5.5	2.79 ± 0.39	3.02 ± 0.48				
	16.5	6.97 ± 0.62	7.61 ± 0.61				

Table 5. Heterogeneity of photobleaching of GFP. Differences between the distribution of magnitude of residuals in illuminated samples and in the control (i.e. a sample illuminated with a nonbleaching dose of light) expressed as Chi-square (significance levels are given in parenthesis).

Excitation light flux ($W\ cm^{-2}$)	Air	Argon
0.6	< 3 (< 0.001)	< 3 (< 0.001)
1.7	< 3 (< 0.001)	15 (0.088)
5.5	9 (0.003)	9 (0.003)
16.5	38 (0.963)	62 (> 0.999)

be a useful way of protecting fluorescent signals in microscopy, with the greatest benefits occurring with low photon fluxes for PI, and high photon fluxes for CA_3.

In order to demonstrate the potential of anoxic imaging in protecting fluorescence signals we imaged the same specimen – a metaphase plate stained with PI (Fig. 5A) – first under anoxic, nonbleaching conditions (Fig. 5B) and subsequently under standard imaging conditions (i.e. in equilibrium with air; Fig. 5C). The image collected under argon contains 3D information from the whole metaphase plate, including the side most distant from the coverslip and the lens. Deterioration of image quality along the *z* axis is due to spherical aberration and light scatter – inevitable problems associated with using an oil immersion lens to image deep into water-containing biological material. No loss of fluorescence signal was detected during data collection. When the same object was imaged again in air, bleaching occurred and the confocal planes recorded at the end of the experiment (i.e. far from the coverslip) contained no detectable signal. As a result, information from part of the metaphase plate is entirely missing.

Dependence of photobleaching on photon flux

Our data indicate that bleaching depends on photon flux, both in the presence and absence of oxygen. This rule holds for the two probes strongly bound to chromatin, PI (Fig. 2G) and eGFP (Fig. 4I). The data in Fig. 4(E) and (F) clearly indicate that signal loss is considerable at the intensities of light used typically for imaging (i.e. 1.7 $W\ cm^{-2}$). However, it is possible to collect images using lower fluxes that minimize bleaching. To prove this point we imaged metaphase plates in cells expressing H2B-eGFP, using low and intermediate photon fluxes (Fig. 6). The image collected using the low photon flux contains more information derived from the side most distant from the coverslip, as compared with the image registered using a high photon flux. The signal-to-noise ratios of the images were 30 dB at low photon flux (Fig. 6B) and 40 dB at high photon flux (Fig. 6C). Thus, the increase of image quality (i.e. signal-to-noise ratio) was as predicted on the basis of a bleaching reaction characterized by the order greater than 1 (Hirschfeld, 1976; Song *et al.*, 1997).

Discussion

Our aim was to investigate the kinetics of photobleaching of some fluorescent probes commonly used in biological imaging – propidium iodide (PI), chromomycin A_3 (CA_3), and an enhanced version of the green fluorescent protein (eGFP) – and to explore whether fading could be reduced by anoxia.

Mechanisms of photobleaching

Propidium iodide. PI binds to DNA mainly through intercalation (Blackburn & Gait, 1996). Furthermore, one may postulate

that in our system PI associates also with external sites, similarly to its structural analogue, ethidium bromide (Bugs & Cornelio, 2002). PI is initially bleached rapidly and then more slowly (Fig. 1A, curve 1), and only the latter phase is reduced significantly by anoxia (Fig. 2B, curve 11). It is attractive to suppose that the fast and slow phases involve populations of molecules, which are externally bound (a minority) and intercalated (the majority).

Only ~10% PI fluorescence is lost during the fast phase. Then, either the bleached subpopulation represents the minority of DNA-bound PI or the fluorescence quantum efficiency of this form of the dye is relatively low. The fast phase is saturated with light intensity (Fig. 2A and B) and has an order of reaction < 1 with respect to PI, under air or argon (Fig. 2E and F), suggesting that excited molecules are long lived. This, indeed is plausible, as it is known that the fluorescence lifetimes of PI and its structural analogues are affected by their mode of binding to DNA (Araki & Yamada, 1985; Radu *et al.*, 1997; Sailer *et al.*, 1996) and the fluorescence lifetime of intercalated EB is 25 ns and 17 ns for the externally bound form (Olmsted & Kearns, 1977; Brown *et al.*, 1991), whereas the quantum efficiency is 0.87 and 0.04, respectively (Bugs & Cornelio, 2002). Thus, it follows that the lifetime of an excited state of an externally bound EB is longer than the intercalated form. The same may hold for PI, as it is also known that the mean fluorescence lifetimes of EB and PI bound to DNA are similar (Cosa *et al.*, 2001).

The excited state nonintercalated fraction of EB and PI is deactivated primarily by deprotonation (Brown *et al.*, 1991; Cosa *et al.*, 2001; Bugs & Cornelio, 2002). Fluorescence plays only a minor role in deactivation, as can be expected from a low quantum efficiency. Following deprotonation, a molecule returns to a ground state and accepts a proton again. This pathway constitutes reversible bleaching and may be limited by the accessibility of proton acceptors. A long lifetime of the excited state of externally bound PI could allow several types of reactions to occur. This notion is in agreement with multiple reactions indicated by the bleachmaps (Tables 1–5). As oxygen appears to be involved only at high light intensities (in the fast phase, Fig. 2A and B), it seems likely that the rate of

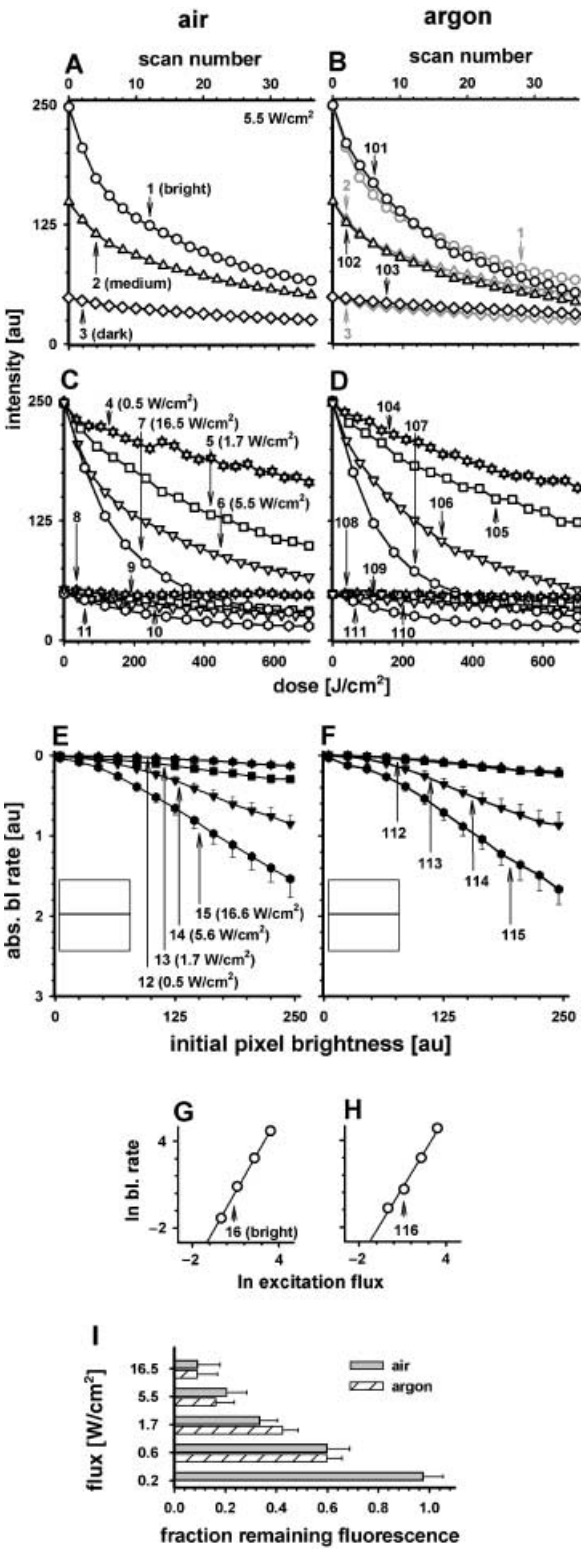

Fig. 4. Kinetics of photobleaching of eGFP bound to chromatin in air (A, C, E, G) or argon (B, D, F, H). The general approach was as described in Fig. 1, except that one scan forms one image. (A), (B) Argon has little effect on bleaching. As in Fig. 1(A) and (B) only three brightness classes are shown for clarity. Means of three experiments. (C), (D) Effect of four different photon fluxes on bleaching. Effects on only bright (curves 4–7 and 104–107) and dim pixels (curves 8–11, 108–111) are shown for clarity. (E), (F) Bleaching rates for bright pixels. Reaction orders are higher than 1 under air and argon. No saturation occurs. (G), (H) Absolute rates of bleaching as a function of initial pixel brightness, for four excitation intensities. Error bars: 95% confidence intervals. Insets: schematics showing normalized bleaching rates as a function of initial pixel brightness. Oxygen does not affect absolute bleaching rates. (I) Fraction of fluorescence remaining on delivery (under air or argon) of the same total dose of light, delivered in laser beams of different photon fluxes. Laser beams of different intensities (i.e. passing through neutral density filters) were used and the total time of illumination was adjusted to deliver the same total dose of light to the sample. Error bars: 95% confidence intervals. A given dose of light causes significantly less photobleaching if delivered at a low photon flux.

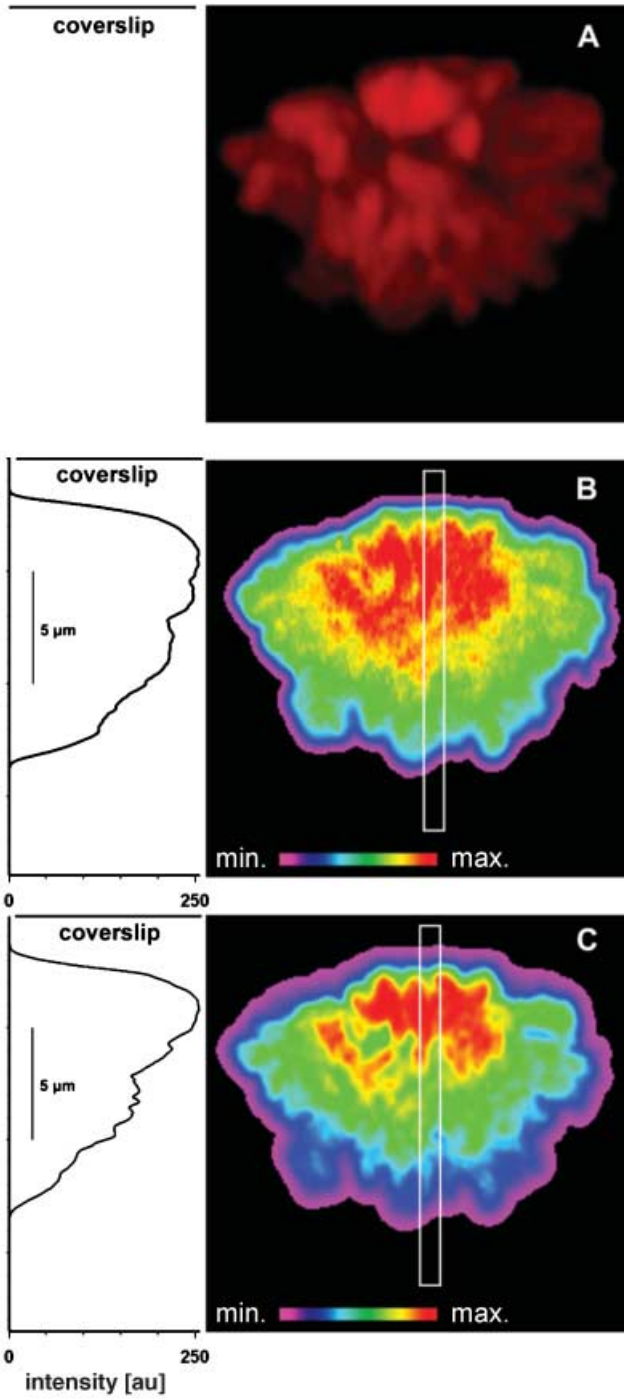

Fig. 5. Anoxic imaging protects the fluorescent signals and facilitates collection of full 3D data sets. 3D images collected in argon (A, B) or in air (C) of chromatin in a cell in mitosis, with condensed chromosomes stained with propidium. Images are projections (in *x*–*z* plane) of 69 consecutive (330 nm) *x*–*y* sections each collected using an average excitation flux of 11 W cm^{-2} in the focal plane. (A) Back-to-front alpha blending projection. (B), (C) Maximum intensity projections (right) and fluorescence (left) measured along the area indicated in the image by a white vertical bar. The intensity in a part of the image distant from the coverslip is lower under air due to photobleaching. The colour bar indicates colours assigned to pixel brightness.

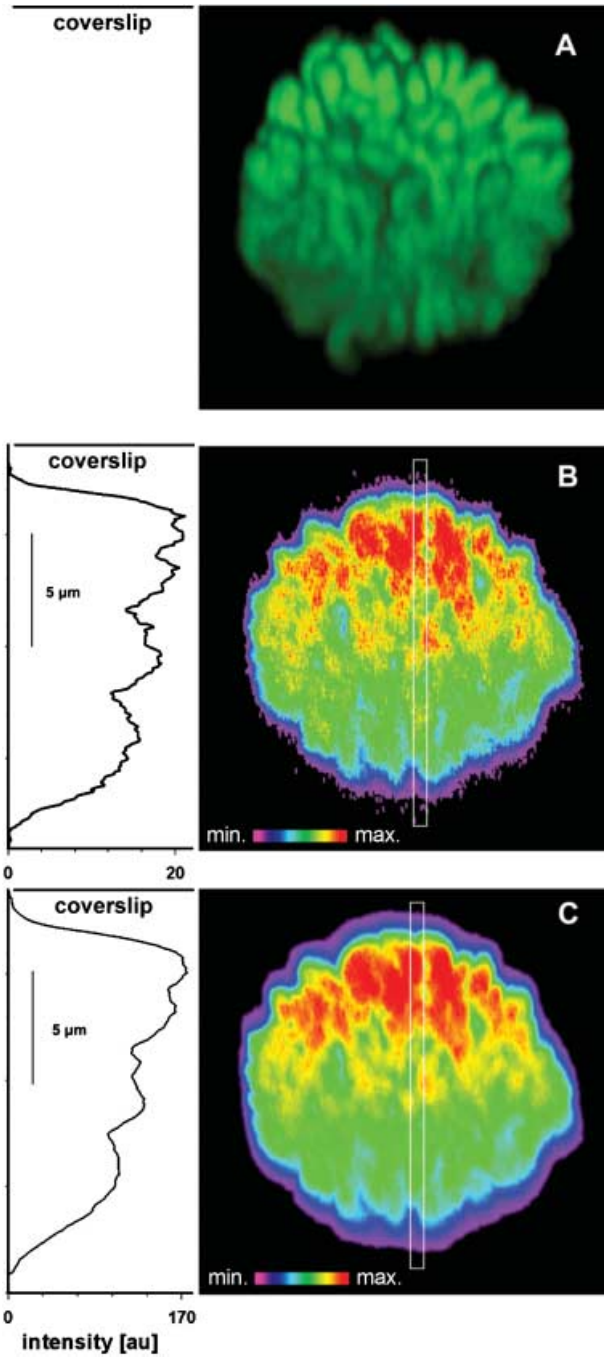

Fig. 6. Low photon flux imaging protects fluorescence of eGFP and results in more fine detail in a 3D image. 3D images of eGFP bound to chromatin in a cell in mitosis, generated using the same total dose of light; the light was delivered in a laser beam of low (0.17 W cm^{-2}, A, B) and intermediate (1.71 W cm^{-2}, C) intensity. The images are projections (in the *x*–z plane) of the set of 65 consecutive *x*–*y* sections. (A) Back-to-front alpha blending projection. (B), (C) Maximum intensity projections (right) and fluorescence (left) measured along the area indicated in the image by a white vertical bar. The initial intensities of fluorescence at low photon flux are approx. eight times lower than at high photon flux, yet more details in a part of the image distant from the coverslip can be resolved. The colour bar indicates colours assigned to pixel brightness.

reactions of PI with oxygen (i.e. D–O) was low in comparison with reactions involving PI and species other than oxygen (i.e. D–X).

Most PI fluorescence is lost during the slow phase. Then either the bleached subpopulation represents the majority of DNA-bound PI or the fluorescence quantum efficiency of this form of the dye is relatively high. The slow phase is not saturable with light (Fig. 2C and D), suggesting that excited molecules are short lived. This is to be expected of intercalative binding. The order of reaction of the slow phase was 3.2 in argon and 1.5 under air (Fig. 2E and F). Thus, one may postulate that slow-phase bleaching was a superposition of a first-order D–O reaction and higher-order D–X reactions. On the other hand, the high order of D–X reactions implies that several molecules of PI are involved in one bleaching event. This notion is in disagreement with the observation that bleaching rates are (with one exception) a linear function of initial pixel brightness, which reflects local PI concentration. A linear dependence on PI concentration of bleaching would imply involvement of only one PI molecule in each bleaching event. Thus, one has to assume that either two-photon excitation of a molecule was observed or the effective local concentration of PI within nanometre-size pixels was the same in bright and dim areas of confocal images. The former notion is unlikely because the exciting flux was low (11–110 W cm^{-2}); the latter is impossible to verify through optical imaging due to the limited resolution, where pixels are hundreds of nanometres across. However, the latter is plausible, as PI binds to naked DNA stoichiometrically. We hypothesize that most photoreacting molecules are bound on the same DNA strand, in close proximity. This idea is supported by the photoinduced transfer of electrons between other bound intercalators (i.e. ethidium bromide, acridine orange) through DNA bases (Brun & Harriman, 1992). Moreover, the fact that, under anoxia, the slow phase bleaching occurs only at high photon fluxes (Fig. 2D), but not at low or intermediate, is in agreement with the hypothesis that groups rather than single molecules of PI are involved in bleaching. One might imagine that a simultaneous excitation of several PI molecules lying in close proximity along the DNA strand can occur only at high photon fluxes.

To conclude, we suggest that the two populations of bound PI are bleached in different ways, and this is reflected by two phases in the kinetics.

Chromomycin A_3

CA_3 binds to a minor groove of DNA either as a dimer (Blackburn & Gait, 1996; Gao & Patel, 1989a,b, 1990) or monomer (Aich *et al.*, 1992; Stankus *et al.*, 1992) complexed with a divalent cation (Mg^{2+}, Zn^{2+}). The loss of CA_3 fluorescence may be adequately described by first-order kinetics, in the absence as well as presence of oxygen (Fig. 3E and F; Tables 3–5). However, whereas oxygen-independent reactions saturate with light intensity, reactions involving oxygen do not (Fig. 3B and C). This is consistent with bleaching occurring from a long-lived triplet state. It addition, only one CA_3 molecule at a time takes part in a bleaching reaction (Tables 3–5); this indicates that, although CA_3 can bind as a dimer, it was bound predominantly as a monomer under our conditions (Aich *et al.*, 1992; Stankus *et al.*, 1992).

Enhanced green fluorescent protein

eGFP was covalently linked to histone H2B, which in turn was bound to DNA (Kanda *et al.*, 1998); therefore, the label was positioned outside the DNA helix. The apparent order of photobleaching of eGFP is > 1, both in the presence and absence of oxygen (Fig. 4E–H). This could be due to the superposition of uni- and bi-molecular reactions involving only eGFP. However, the kinetics appears to be a linear function of the local eGFP concentration (Fig. 4A and B), so they may be explained differently. One may postulate that two-photon excitation of GFP was responsible for the high order of photobleaching reactions observed in our system. However, the incident flux was too low (i.e. 0.6–16.5 W cm^{-2}) to cause two-photon bleaching, which depends (at least) on the square of excitation power (Chen *et al.*, 2002). GFP and eGFP have several distinct excitation states that can interconvert (Chattoraj *et al.*, 1996; Brejc *et al.*, 1997; Pierce *et al.*, 1997; Haupts *et al.*, 1998; Tsien, 1998; Harms *et al.*, 2001). The eGFP we used does not exhibit long-term reversible photoconversion, and we saw no green to red conversion (not shown; Elowitz *et al.*, 1997); however, fast relaxation has been reported (Chattoraj *et al.*, 1996; Weber *et al.*, 1999). Assuming that the latter occurs in our system, one can postulate that eGFP might absorb (from anionic and zwitterionic ground states) two photons at high exciting fluxes, and so be bleached irreversibly. Consequently, we suggest that bleaching of eGFP is unimolecular (with respect to eGFP), but may involve multiple excited states to give the nonlinear dependence of bleaching rate on excitation intensity.

Oxygen did not influence the bleaching of eGFP (Fig. 4G–I). This is consistent with the chromophore being shielded from oxygen (Prendergrast, 1999). Similar behaviour was reported in the case of R-phycoerythrin (White & Stryer, 1987), where the fluorophores are embedded in protein moiety. However, exciting GFP can lead to the production of singlet oxygen (Greenbaum *et al.*, 2000), which suggests that energy must be transferred from the chromophore to dissolved oxygen; clearly, this reaction requires further investigation.

Anoxic imaging and antifade agents

Agents such as NPG (N-propyl gallate), DABCO (1,4-diazabicyclo[2.2.2]octane), 4-POBN (α-(4-Pirydyl-1-oxide)-N-*tert*-butyl nitrone) and PPD (P-phenylanediamine) reduce bleaching and are often added as 'antifade' reagents to mounting media. However, they also reduce the intensity of the

initial signal (White *et al.*, 1987; Longin *et al.*, 1993; Song *et al.*, 1996). They may also be of little use with DNA-binding dyes, as they and their solvents, which are both nonpolar, may interfere with dye binding. For example, Vectashield (which contains PPD in buffered glycol; Longin *et al.*, 1993) reduces the signal of PI bound to DNA, whereas NPG in 80% glycerol eliminates the red luminescence from RNA in cells stained with acridine orange (not shown). In contrast, anoxia minimizes, and sometimes eliminates, the bleaching of DNA-bound dyes, without detectable effect on cell structure. Moreover, it may also protect cell structures from direct destruction by exciting light. In addition, oxygen is a collisional quencher of fluorescence, so anoxia increases fluorescence, as observed with fluorescein in solution, or PI bound to DNA (not shown). However, removing oxygen may change the apparent order of reaction; thus, an increase in signal-to-noise ratio may be achieved only under optimal imaging conditions (discussed further).

Photobleaching vs. photon flux

Several investigators reported that bleaching of fluorophores in a point scanning microscope was most intense in a confocal plane (White *et al.*, 1987; Nagelhus *et al.*, 1996; Van Oostveldt *et al.*, 1998). As the total dose of light delivered to the adjacent planes is roughly the same, but the dose-rate is lower, Tsien & Waggoner (1995) suggested that the bleaching is faster in areas receiving the peak intensities of light. This could imply that, in microscopy for the same dose, bleaching may be faster when photon flux is greater. Our data presented here (Figs 2G and 4I) provide further support in favour of this notion.

It is worth noting that, in the case of PI (predominant binding mode, slow phase photobleaching), the D–X reactions appear to be absent when the sample is exposed to low photon flux (Fig. 2C and D). Under these conditions photobleaching of PI bound to DNA seems to proceed exclusively via D–O reactions. Thus, at low photon flux, removal of oxygen can eliminate the slow phase photobleaching entirely. As the photon flux increases, the D–X reactions occupy a growing proportion of photobleaching reactions (Fig. 1C and D). In other words, it appears to be possible to manipulate the ratio between D–X and D–O reactions by altering the photon flux.

One may argue that excitation of fluorochromes using high fluxes of light (which is common in confocal microscopy) may cause saturation of the excited state. Indeed, in the case of eGFP, saturation of the fluorescence (i.e. the first excited singlet state) might occur when the bleaching beam of the highest instantaneous flux is used (Harms *et al.*, 2001). However no saturation of photobleaching rates was observed in our experiments. It seems plausible that other (singlet) excited states, which are not deactivated through fluorescence, contribute to photobleaching. One may estimate that in the case of PI excited using bleaching beam of the highest intensity only 5–10% of dye molecules would reside in the singlet excited state, provided that stationary conditions were reached. Thus, it seems unlikely that saturation of the singlet excited state could influence PI photobleaching in our experiments. Unfortunately, no data on the saturation of excited state of CA_3 are available. Nonetheless, one may note that CA_3 was only weakly excited using 457 nm light in our experiments.

The observed dependence of photobleaching rates on photon flux could be an artefact arising from saturation of the light detector. Approximately 20, 1 and 0.5 photons on average were collected per scan for eGFP, PI and CM_3, respectively. Thus, saturation might have occurred only in the brightest pixels of eGFP images. However, such a saturation probably did not occur as the kinetics of bleaching of the brightest and dimmer classes of pixels did not differ and the rates of photobleaching depended linearly on pixel brightness.

One can argue that lower photobleaching rates of PI and eGFP observed at low photon fluxes suggest that a tangible progress in confocal microscopy could be achieved by employing light detectors of higher quantum efficiency and lower dark current. This, in practice, may be interpreted as an indication that a wide-field fluorescence microscope equipped with a sensitive CCD camera and deconvolution software or a multiple beam scanning confocal device might be more likely to allow less photobleaching and thus a better quality of a final image. The latter conclusion seems premature though, as a number of other factors besides photobleaching need to be optimized in these systems to achieve improved imaging conditions.

Practical advice when imaging

Although numerical models allowing mathematical correction for signal loss are available (Nagelhus *et al.*, 1996), it seems unlikely that any unified approach will provide accurate and general solutions, simply because the bleaching kinetics are so complicated. There also seem to be few practical guidelines that can be given, even for many commonly used dyes (Florijn *et al.*, 1995; Patterson *et al.*, 1997; Song *et al.*, 1997; Van Oostveldt *et al.*, 1998; Kunz & MacRobert, 2002). If corrections are to be made, it seems that a specific model must be designed for each bound fluorophore studied (Kanony *et al.*, 2001). Suitable algorithms may be constructed provided that the fluorophore is bound tightly to labelled structure and exhibits monophasic kinetics of photobleaching. Our data pertinent to photobleaching of eGFP provide a basis for such a correction routine. It seems clear that with PI and CA_3, removing oxygen slows or even eliminates bleaching; therefore, our general conclusion is that anoxia is likely to yield better images with these dyes. However, no improvements can be expected with eGFP, as this fluorophore seems to be protected from oxygen by nature.

What practical strategies should be used to obtain the highest signal-to-noise ratio? The total number of photons emitted by an ensemble of fluorescent molecules (integrated emission)

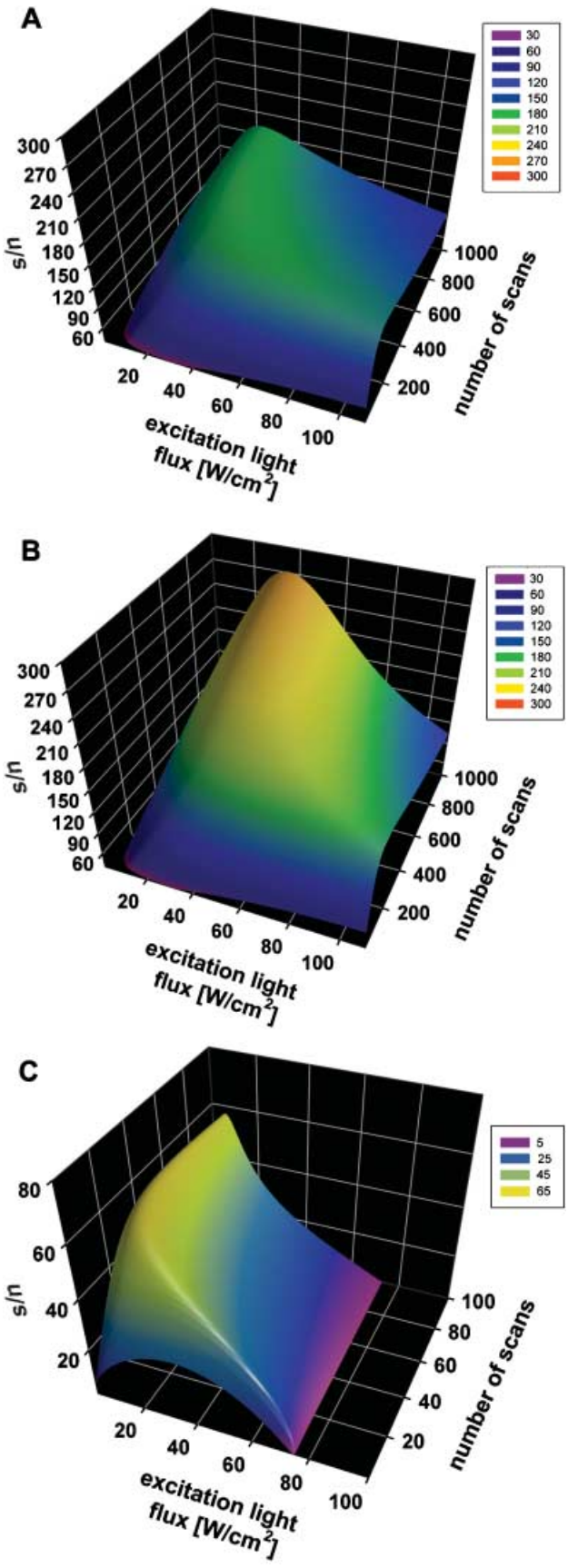

depends on the flux of excitation light and a photobleaching constant (k_b), which is influenced by the presence of oxygen. Consequently, the optimal signal-to-noise ratio can be achieved only at a certain value of excitation light flux and image acquisition time (or the number of frames collected), as indicated by the numerical model illustrated in Fig. 7(A)–(C). On one hand, for high-order reactions (e.g. involving eGFP and intercalated PI) it is advantageous to use a long image acquisition time (or accumulate a large number of frames) while keeping the exciting flux low. On the other hand, for (rare) reactions with order close to unity, the opposite strategy produces the highest signal-to-noise ratio. For most fluorophores (which are characterized by high order bleaching reactions), the dependence on photon flux of signal loss suggests that delivering the dose required for image acquisition will yield a better signal stability, a higher signal-to-noise ratio, and so a better image if it is divided into the smallest possible portions, with averaging of the resulting images. Then, the claimed lower bleaching rates in wide-field and multipoint scanners (compared to point-scanning confocals) may be explained by the lower dose rates used in the former instruments. Low photon fluxes may also be advantageous for live cell imaging (Manders *et al.*, 2003).

Removing oxygen from the vicinity of a fluorophore, either by displacing it with argon (as with PI, above) or by wrapping a protective protein shield around the fluorophore (as with eGFP), provide excellent ways of preventing photooxidation. Eliminating oxygen-dependent reactions with anoxia, and avoiding D–X reactions using low-intensity excitation (with eGFP and intercalated PI) yield the highest signal-to-noise ratios and so the best resolution. Particular fluorophores also require particular approaches; for example, when collecting 3D images of PI bound to DNA, it would be best to acquire image data under argon, let the fast-bleaching component vanish first, and then work with the stable signal thereafter.

In summary, we conclude that anoxia protects cell structure from direct photodynamic damage. It also protects fluorescence signals from all dyes studied (except eGFP), and it improves initial signals by eliminating collisional quenching by oxygen. However, we can propose no general model for photobleaching, or provide any simple mathematical corrections. Rather,

Fig. 7. Optimizing imaging conditions. The quality (signal-to-noise ratio, s/n) of an image of a fluorescently labelled structure depends on the number of scans used to generate the image, and the intensity of exciting light (and so the kinetics of bleaching). The interrelationship between the flux of exciting light (in the focal plane), a number of scans, and the resultant signal-to-noise ratio was calculated using the model described in Materials and methods. The value of the signal-to-noise ratio is shown in the colour scale. Three cases were modelled: PI in equilibrium with air (A, where bleaching is a combination of fast low-order and slow high-order reactions), PI in anoxic conditions (B, where bleaching is mainly due to a fast low-order reaction), and eGFP in equilibrium with air (C, where high-order fast reactions dominate).

the optimal strategy for image collection depends on the bleaching kinetics of the particular fluorophore used, and, for high-order reactions, anoxic imaging combined with a low photon flux gives a stable signal and the best images.

Acknowledgements

This work was supported by The Wellcome Trust (IRDA grant to P.R.C. and J.W.D.) and Polish State Committee for Scientific Research (J.D.D., grant 0278/P04/2001/21). We acknowledge excellent technical assistance by Barbara Czuba-Pelech, Eng. In preparing this work we benefited from helpful discussions with Professor F. Brakenhoff, Dr E. Manders (J.W.D.) and Professor J. Maluszynska (T.B.).

References

Abuknesha, R.A., al-Mazeedi, H.M. & Price, R.G. (1992) Reduction of the rate of fluorescence decay of FITC- and carboxyfluorescein- stained cells by anti-FITC antibodies. *Histochem. J.* **24**, 73–77.

Aich, P., Sen, R. & Dasgupta, D. (1992) Role of magnesium ion in the interaction between chromomycin A_3 and DNA: binding of chromomycin A_3-Mg^{2+} complexes with DNA. *Biochemistry*, **31**, 2988–2997.

Araki, T. & Yamada, M. (1985) Fluorescence decay measurements for determining the relative content of ethidium bromide to DNA in situ in cell nuclei. *Histochemistry*, **83**, 299–301.

Blackburn, G.M. & Gait, J.M. (1996) *Nucleic Acids in Chemistry and Biology*. Oxford University Press, Oxford.

Brakenhoff, G.J., Visscher, K. & Gijsbers, E.J. (1994) Fluorescence bleach rate imaging. *J. Microsc*, **175**, 154–161.

Brejc, K., Sixma, T.K., Kitts, P.A., Kain, S.R., Tsien, R.Y., Ormo, M. & Remington, S.J. (1997) Structural basis for dual excitation and photoisomerization of the *Aequorea victoria* green fluorescent protein. *Proc. Natl. Acad. Sci. USA*, **94**, 2306–2311.

Brown, D.W., Libertini, L.J. & Small, E.W. (1991) Fluorescence anisotropy decay of ethidium bound to nucleosome core particles. 1. Rotational diffusion indicates an extended structure at low ionic strength. *Biochemistry*, **30**, 5293–5303.

Brun, A.M. & Harriman, A. (1992) Dynamics of electron transfer between intercalated polycyclic molecules: effect of interspersed bases. *J. Am. Chem. Soc*. **114**, 3656–3660.

Bugs, R. & Cornelio, M.L. (2002) A new biophysics approach using photoacoustic spectroscopy to study the DNA–ethidium bromide interaction. *Eur Biophys. J*. **31**, 232–240.

Chattoraj, M., King, B.A., Bublitz, G.U. & Boxer, S.G. (1996) Ultra-fast excited state dynamics in green fluorescent protein: multiple states and proton transfer. *Proc. Natl. Acad. Sci. USA*, **93**, 8362–8367.

Chen, T.S., Zeng, S.Q., Luo, Q.M., Zhang, Z.H. & Zhou, W. (2002) High-order photobleaching of green fluorescent protein inside live cells in two-photon excitation microscopy. *Biochem. Biophys. Res. Commun*, **291**, 1272–1275.

Cosa, G., Focsaneanu, K.S., McLean, J.R., McNamee, J.P. & Scaiano, J.C. (2001) Photophysical properties of fluorescent DNA-dyes bound to single- and double-stranded DNA in aqueous buffered solution. *Photochem. Photobiol*. **73**, 585–599.

Darzynkiewicz, Z. & Kapuscinski (1990) Acridine orange: a versatile probe of nucleic acids and other cell constituents. *Flow Cytometry and Sorting 2* (ed. by M. R. Melamed, M. L. Mendelson and T. Lindmo), pp. 291–314. Wiley-Liss, New York.

Dobrucki, J.W. (2001) Interaction of oxygen-sensitive luminescent probes $Ru(phen)_{(3)}^{(2+)}$ and $Ru(bipy)_{(3)}^{(2+)}$ with animal and plant cells in vitro. Mechanism of phototoxicity and conditions for non-invasive oxygen measurements. *J. Photochem. Photobiol. B*, **65**, 136–144.

Elowitz, M.B., Surette, M.G., Wolf, P.E., Stock, J. & Leibler, S. (1997) Photoactivation turns green fluorescent protein red. *Curr. Biol*. **7**, 809–812.

Florijn, R.J., Slats, J., Tanke, H.J. & Raap, A.K. (1995) Analysis of antifading reagents for fluorescence microscopy. *Cytometry*, **19**, 177–182.

Gao, X.L. & Patel, D.J. (1989a) Antitumour drug–DNA interactions: NMR studies of echinomycin and chromomycin complexes. *Q Rev. Biophys*. **22**, 93–138.

Gao, X.L. & Patel, D.J. (1989b) Solution structure of the chromomycin-DNA complex. *Biochemistry*, **28**, 751–762.

Gao, X.L. & Patel, D.J. (1990) Chromomycin dimer-DNA oligomer complexes. Sequence selectivity and divalent cation specificity. *Biochemistry*, **29**, 10940–10956.

Giloh, H. & Sedat, J.W. (1982) Fluorescence microscopy: reduced photobleaching of rhodamine and fluorescein protein conjugates by n-propyl gallate. *Science*, **217**, 1252–1255.

Greenbaum, L., Rothmann, C., Lavie, R. & Malik, Z. (2000) Green fluorescent protein photobleaching: a model for protein damage by endogenous and exogenous singlet oxygen. *Biol. Chem*. **381**, 1251–1258.

Harms, G.S., Cognet, L., Lommerse, P.H., Blab, G.A. & Schmidt, T. (2001) Autofluorescent proteins in single-molecule research: applications to live cell imaging microscopy. *Biophys. J*. **80**, 2396–2408.

Haupts, U., Maiti, S., Schwille, P. & Webb, W.W. (1998) Dynamics of fluorescence fluctuations in green fluorescent protein observed by fluorescence correlation spectroscopy. *Proc. Natl. Acad. Sci. USA*, **95**, 13573–13578.

Hirschfeld, T. (1976) Quantum efficiency independence of the time integrated emission from a fluorescent molecule. *Appl. Opt*, **15**, 3135–3139.

Kanda, T., Sullivan, K.F. & Wahl, G.M. (1998) Histone-GFP fusion protein enables sensitive analysis of chromosome dynamics in living mammalian cells. *Curr. Biol*. **8**, 377–385.

Kanony, C., Akerman, B. & Tuite, E. (2001) Photobleaching of asymmetric cyanines used for fluorescence imaging of single DNA molecules. *J. Am. Chem. Soc*. **123**, 7985–7995.

Koppel, D.E. (1986) Fluorescence photobleaching recovery techniques for translational and slow rotational diffusion in solution and on cell surfaces. *Biochem. Soc. Trans*. **14**, 842–845.

Kunz, L. & MacRobert, A.J. (2002) Intracellular photobleaching of 5,10,15,20-tetrakis (m-hydroxyphenyl) chlorin (Foscan) exhibits a complex dependence on oxygen level and fluence rate. *Photochem. Photobiol*. **75**, 28–35.

Lindqvist, L. (1960) A flash photolysis study of fluorescein. *Arkiv Kemi*. **16**, 79–138.

Longin, A., Souchier, C., Ffrench, M. & Bryon, P.A. (1993) Comparison of anti-fading agents used in fluorescence microscopy: image analysis and laser confocal microscopy study. *J. Histochem. Cytochem*. **41**, 1833–1840.

Manders, E.M., Visser, A.E., Koppen, A., de Leeuw, W.C., van Liere, R., Brakenhoff, G.J. & van Driel, R. (2003) Four-dimensional imaging of chromatin dynamics during the assembly of the interphase nucleus. *Chromosome Res*. **11**, 537–547.

Morgan, T.L., Yang, D.J., Fry, D.G., Hurlin, P.J., Kohler, S.K., Maher, V.M. & McCormick, J.J. (1991) Characteristics of an infinite life span diploid human fibroblast cell strain and a near-diploid strain arising from a clone of cells expressing a transfected v-myc oncogene. *Exp. Cell Res*. **197**, 125–136.

Nagelhus, T.A., Slupphaug, G., Krokan, H.E. & Lindmo, T. (1996) Fading correction for fluorescence quantitation in confocal microscopy. *Cytometry*, **23**, 187–195.

Olmsted, J. III & Kearns, D.R. (1977) Mechanism of ethidium bromide fluorescence enhancement on binding to nucleic acids. *Biochemistry*, **16**, 3647–3654.

Patterson, G.H., Knobel, S.M., Sharif, W.D., Kain, S.R. & Piston, D.W. (1997) Use of the green fluorescent protein and its mutants in quantitative fluorescence microscopy. *Biophys. J*. **73**, 2782–2790.

Patterson, G.H. & Piston, D.W. (2000) Photobleaching in two-photon excitation microscopy. *Biophys. J*. **78**, 2159–2162.

Pawley, J. (1995) Fundamental limits in confocal microscopy. *Handbook of Biological Confcocal Microscopy* (ed. by J. B. Pawley), pp. 19–37. Plenum Press, New York.

Peters, R., Peters, J., Tews, K.H. & Bahr, W. (1974) A microfluorimetric study of translational diffusion in erythrocyte membranes. *Biochim. Biophys. Acta*, **367**, 282–294.

Phair, R.D. & Misteli, T. (2000) High mobility of proteins in the mammalian cell nucleus. *Nature*, **404**, 604–609.

Pierce, D.W., Hom-Booher, N. & Vale, R.D. (1997) Imaging individual green fluorescent proteins. *Nature*, **388**, 338.

Prendergast, E.G. (1999) Biophysics of the green fluorescent protein. *Green Fluorescent Proteins* (ed. by K. F. Sullivan and S. A. Kay). *Meth. Cell Biol*. **58**, 1–18.

Radu, L., Preoteasa, V., Radulescu, I. & Radu, S. (1997) Fluorescence lifetime, precision calorimetry, and fluorescence energy transfer measurements in the study of normal and tumoral chromatin structure. *J. Mol Struct*. **408/409**, 191–194.

Sailer, B.L., Nastasi, A.J., Valdez, J.G., Steinkamp, J.A. & Crissman, H.A. (1996) Interactions of intercalating fluorochromes with DNA analyzed by conventional and fluorescence lifetime flow cytometry utilizing deuterium oxide. *Cytometry*, **25**, 164–172.

Song, L., Hennink, E.J., Young, I.T. & Tanke, H.J. (1995) Photobleaching kinetics of fluorescein in quantitative fluorescence microscopy. *Biophys. J*. **68**, 2588–2600.

Song, L., van Gijlswijk, R.P., Young, I.T. & Tanke, H.J. (1997) Influence of fluorochrome labeling density on the photobleaching kinetics of fluorescein in microscopy. *Cytometry*, **27**, 213–223.

Song, L., Varma, C.A., Verhoeven, J.W. & Tanke, H.J. (1996) Influence of the triplet excited state on the photobleaching kinetics of fluorescein in microscopy. *Biophys. J*. **70**, 2959–2968.

Stankus, A., Goodisman, J. & Dabrowiak, J.C. (1992) Quantitative footprinting analysis of the chromomycin A3–DNA interaction. *Biochemistry*, **31**, 9310–9318.

Stelzer, E.H.K. (1998) Contrast, resolution, pixelation, dynamic range and signal to noise ratio: fundamental its to resolution in fluorescence light microscopy. *J. Microsc*, **189**, 15–24.

Szabo, G. Jr, Pine, P.S., Weaver, J.L., Kasari, M. & Aszalos, A. (1992) Epitope mapping by photobleaching fluorescence resonance energy transfer measurements using a laser scanning microscope system. *Biophys. J*. **61**, 661–670.

Tanhuanpaa, K., Virtanen, J. & Somerharju, P. (2000) Fluorescence imaging of pyrene-labeled lipids in living cells. *Biochim. Biophys. Acta*, **1497**, 308–320.

Tossi, A.B. & Kelly, J.M. (1989) A study of some polypyridylruthenium (II) complexes as DNA binders and photocleavage reagents. *Photochem. Photobiol*. **49**, 545–556.

Tsien, R.Y. (1998) The green fluorescent protein. *Annu. Rev. Biochem*. **67**, 509–544.

Tsien, R.Y. & Waggoner (1995) Fluorophores for Confocal Microscopy. Photophysics and Photochemistry. *Handbook of Biological Confocal Microscopy 2* (ed. by J. B. Pawley), pp. 267–279. Plenum Press, New York.

Usui, Y., Itoh, K. & Koizumi, M. (1965) Switch-over of the mechanism of primary processes in the photo-oxidation of xanthene dyes as revealed by the oxygen consumption experiments. *Bull. Chem. Soc. Jpn* **38**, 1015–1022.

Van Oostveldt, P., Verhaegen, F. & Messens, K. (1998) Heterogeneous photobleaching in confocal microscopy caused by differences in refractive index and excitation mode. *Cytometry*, **32**, 137–146.

Weber, W., Helms, V., McCammon, J.A. & Langhoff, P.W. (1999) Shedding light on the dark and weakly fluorescent states of green fluorescent proteins. *Proc. Natl. Acad. Sci. USA*, **96**, 6177–6182.

White, J.G., Amos, W.B. & Fordham, M. (1987) An evaluation of confocal versus conventional imaging of biological structures by fluorescence light microscopy. *J. Cell Biol*. **105**, 41–48.

White, J.C. & Stryer, L. (1987) Photostability studies of phycobiliprotein fluorescent labels. *Anal. Biochem*. **161**, 442–452.